Hingepoints and neural folds reveal conserved features of primary neurulation in the zebrafish forebrain

Jonathan M. Werner[1], Maraki Y. Negesse[1], Dominique L. Brooks[1], Allyson R. Caldwell[1], Jafira M. Johnson[1] and Rachel Brewster[1]

1. Department of Biological Sciences, University of Maryland Baltimore County, Baltimore, MD 21250

ABSTRACT

Primary neurulation is the process by which the neural tube, the central nervous system precursor, is formed from the neural plate. Incomplete neural tube closure occurs frequently, yet underlying causes remain poorly understood. Developmental studies in amniotes and amphibians have identified hingepoint and neural fold formation as key morphogenetic events and hallmarks of primary neurulation, the disruption of which causes neural tube defects. In contrast, the mode of neurulation in teleosts like zebrafish has remained highly debated. Teleosts are thought to have evolved a unique pattern of neurulation, whereby the neural plate infolds in absence of hingepoints and neural folds, at least in the hindbrain/trunk where it has been studied. We report here on zebrafish forebrain morphogenesis where we identify these morphological landmarks. Our findings reveal a deeper level of conservation of neurulation than previously recognized and establish the zebrafish as a model to understand human neural tube development.

INTRODUCTION

Primary neurulation is the process by which the neural tube, the precursor of the brain and spinal cord, is shaped from an open single-cell layered epithelium, known as the neural plate. These morphogenetic events have mostly been studied in amniotes (mouse and chick) and amphibians (frogs), where conserved mechanisms were identified. Following neural induction, the neural plate (Figure 1A) narrows and elongates by convergent extension movements [1,2]. The morphology of the neural plate is further changed by bending in a biphasic manner, initiated at hingepoints [3]. The first morphological event is the formation of the medial hingepoint (MHP), which bends the flat neural plate into a V shape, forming the neural groove (Figure 1B). Neural folds at the edges of the neural plate are subsequently elevated by this neuroectoderm-intrinsic force and also by the expansion of the head mesoderm in the cranial region [4]. In the second phase, the neural plate bends and folds at paired dorso-lateral hingepoints (DLHPs), which brings the neural folds closer together (Figure 1C). The neural folds eventually meet and fuse at the dorsal midline, completing neural tube formation. The dorsal midline is subsequently remodeled to separate the inner neuroectoderm from the outer non-neural ectoderm fated to become the epidermis (Figure 1D). In the cranial region of amniotes, neural tube closure is initiated at several sites and extends via a zippering process either in a unidirectional or bidirectional manner from these closure points to seal the neural tube. Incomplete cranial neural tube closure occurs frequently, resulting in anencephaly and exencephaly [3].

Several cellular mechanisms have been identified that contribute to the bending of the neural plate, among which apical constriction is the most studied [5-8]. A meshwork of F-actin accumulates at the apical cortex of neuroectodermal cells and contracts, thereby reducing

the cell apex during neural tube closure (Figure 1b1). The contraction is driven by the molecular motor myosin that co-localizes with F-actin at the apical cortex. Disruption of F-actin using drug inhibitors or in mice deficient for regulators of the cytoskeleton such as Shroom3, the actin-binding protein vinculin or a RhoA-specific GEF (GEF-H1) causes severe cranial neural tube defects [5,9-14]. Similarly, treatment with blebbistatin, an inhibitor of non-muscle myosin II activity, impairs apical constriction of hingepoint cells in the superficial layer of the *Xenopus* neural plate [15].

In contrast to hingepoint formation, the cell intrinsic mechanisms that shape neural fold cells are less understood. The neural folds are bilaminar, consisting of a layer of neuroectoderm capped by a layer of non-neural ectoderm [16]. Neural fold fusion involves the formation of cellular protrusions (filopodia and lamellipodia) that span the midline gap and establish the first contact and attachment points with neural fold cells from the contralateral side [17-19] (Figure 1c1). There is little consensus on the cell type, neuroectoderm or non-neural ectoderm, that generates the cellular protrusions as it varies depending on the species and the axial level. In the mouse forebrain, the initial contact is made by neuroectodermal cells [17,20-23]. Treatment with Cytochalasin D, an inhibitor of actin polymerization or genetic ablation of the cytoskeletal regulators Rac1 or Cdc42 blocks the formation of protrusions and prevents neural fold fusion [19], revealing the central role of these cellular processes.

Though more anterior regions of the neural tube undergo primary neurulation as described above, most vertebrates also exhibit a distinct type of neural tube formation in more posterior regions, termed secondary neurulation. During this process, a mesenchymal cell population condenses into a solid neural rod that subsequently epithelializes and forms a central lumen [24,25]. The mechanisms of neural tube formation in zebrafish have been the

source of considerable debate, and it has been proposed that they are unique among vertebrates [26 27]. In zebrafish, the neural tube in the hindbrain and trunk region initially forms a solid rod (the neural keel) that later develops a lumen, a process seemingly analogous to secondary neurulation [28]. However, examination of the tissue architecture in zebrafish [29-31] and other teleosts [32,33] revealed that the neural rod is shaped by infolding of a neural plate (albeit incompletely epithelialized), which best fits the description of primary neurulation [26]. Despite this evidence, differences in tissue architecture, the mesenchymal-like character of the neural plate and the apparent lack of hingepoints, neural groove and neural folds are difficult to reconcile with a mode of primary neurulation and have contributed to the persistent view that neural tube formation in teleosts is different than in other vertebrates [34-36].

We show here that, in contrast to the zebrafish hindbrain and trunk region, the process of neural tube formation in the forebrain of this teleost exhibits the hallmarks of primary neurulation observed in other vertebrates. We observe the presence of hingepoints and neural folds in the epithelialized anterior neural plate (ANP), demonstrate that formation of the MHP involves oscillatory apical contractions that progressively reduce the apical surface, and show that disruption of myosin function impairs apical constriction of these cells and neural fold convergence. We further show that neural tube closure is initiated at two separate sites in the forebrain and that fusion of the neural folds is mediated by filopodial-like extensions of neuroectodermal cells that bridge the midline. These findings identify conserved mechanisms of primary neurulation that were previously overlooked in teleosts and support the suitability of zebrafish for understanding the etiology of human neural tube defects.

RESULTS

Epithelial character of the anterior neural plate is associated with bending and folding movements

The zebrafish ANP is quite distinct from the neural plate in more posterior regions, as it undergoes precocious epithelialization [37]. To assess whether the epithelialized nature of the ANP also correlates with a change in the mode of neurulation, we examined the morphology of the neuroectoderm in optical cross sections at developmental stages ranging from 2 to 7 somites (som). We observed that at 2-5 som the ANP has a V shape marked by a medial neural groove (black arrowhead) flanked by the elevated lateral edges of the ANP (white arrowhead), which are reminiscent of neural folds (Figure 2A-C). By 6 som the groove is no longer visible and the elevated edges of the ANP have fused medially (Figure 2E, white arrowhead) and form a dorsal bulge by 7 som (Figure 2F, white arrowhead). These observations suggest that the ANP bends and folds around hingepoints to facilitate the medial convergence and fusion of neural folds at the dorsal midline.

The anterior neural plate is multi-layered and gives rise to the eyes and forebrain

The central part of the ANP is fated to become the eyes, while its lateral edges produce the dorsally-located telencephalon and the ventral-most ANP region gives rise to the hypothalamus/ventral diencephalon [37,38]. To gain a better understanding of the morphogenetic events that shape the zebrafish ANP, we examined transverse views of transgenic Tg[*emx3:YFP*] embryos at developmental stages 2, 5, 7 and 10 som, in which telencephalon precursors are labeled with the yellow fluorescent protein (YFP) [39]. We observed, as previously described [37], that the ANP is a multi-layered tissue, with a

mesenchymal superficial core and a marginal or deep layer. These layers will henceforth be referred to as the superficial and deep layers, respectively (s and d in Figure 3A,B). The YFP-positive lateral edges of the ANP elevate, migrate over the eye field and fuse medially at 7 som to form the telencephalon (Figure 3C-D) [37,38]. By 7 som the multilayered ANP (Figure 3A, B) resolves into a single-cell layered neuroectoderm and Ivanovitch et al. (2013)[37] have shown that this process involves radial intercalation of superficial cells between deep marginal cells, which also contributes to the expansion of the optic vesicles (Figure 3F, G). While the morphological changes and cellular dynamics that form the eyes are quite well understood [37,38], the accompanying events that shape the forebrain are for the most part unknown and the focus of the current study.

Structures analogous to hingepoints and neural folds are present in the anterior neural plate

To investigate whether the ANP bends and folds around hingepoints to bring neural folds in close apposition, we examined the cytoarchitecture of this tissue in embryos at stages 2-10 som, labeled with phalloidin (filamentous (F) actin), anti-Sox3 (neural cells) and anti-p63 (epidermal cells, nuclear label) (Figure 3E-H).

We found that at 2 som, neural cells appear mesenchymal with no visible polarized enrichment of F-actin (Figure 3E), consistent with previous observations [37]. The epidermis at this stage is in a far lateral position (white arrowhead in Figure 3E).

Between 2 and 5 som, cells undergo rapid epithelialization, as evidenced by foci of F-actin enrichment in the medial/superficial region (M in Figure 3F, I) and in two dorso-lateral clusters in the deep marginal layer (DL in Figure 3F, I). The apical surfaces of the

146 epithelialized superficial cells appear to constrict and orient towards the midline, resulting in
147 the formation of a medial neural groove (asterisk in Figure 3I). Similarly, the paired dorso-
148 lateral clusters of epithelialized cells in the deep layer are also apically constricted and the
149 neuroectoderm bends and folds sharply at this level (red arrows in Figure 3I), elevating the
150 lateral edges of the ANP above the superficial layer and bringing them closer to the midline.
151 These data suggest that the medial and dorso-lateral cells enriched for apical F-actin may
152 function as hingepoints. Similarly to amphibians whose neural plate is bilayered [40], the
153 putative medial hingepoint in the zebrafish ANP forms in the superficial layer and is therefore
154 more dorsally positioned than its chick and mouse counterpart. However, the zebrafish dorso-
155 lateral hingepoints form in the deep layer.

156 The lateral edges of the ANP are bilaminar at 5 som, consisting of a layer of
157 neuroectoderm cells capped by a layer of p63-positive non-neural ectoderm (and Sox3/p63-
158 negative olfactory placodal cells bridging the two layers), indicative of a neural fold structure
159 (Figure 3F, I). The YFP-positive ANP cells in Tg[*emx3:YFP]* embryos correspond to the
160 neuroectoderm component of neural fold (Figure 3B), revealing that the tip of the neural fold
161 gives rise to the telencephalon. At 4 som, the YFP-positive region of Tg[*emx3:YFP*] embryos
162 extends the length of the forebrain (Figure 2C), delineating the anterior-posterior range of the
163 neural folds.

164 The neural fold and putative hingepoints are transient as they are no longer observed
165 in 7 som embryos. By this stage, the tips of the neural folds have converged medially and
166 fused, forming the telencephalon (Figure 3G). These cells are enriched for apical F-actin at
167 10 som, indicating that they epithelialize (Figure 3D). The non-neural ectoderm still occupies
168 a lateral position at 7 som (Figure 3C, arrowheads), however by 10 som these cells migrate

and fuse dorsally (single arrowhead in Figure 3D), indicating that, as observed in mice, the neuroectodermal component of the neural folds meet first (Figure 1) [20,21]. Measurements of the distance between the medial-most p63-positive domain and the dorsal midline at stages 2-7 som indicate that the non-neural ectoderm portion of the neural folds converges steadily towards the midline and may provide a lateral force that contributes to the displacement of neural folds (Figure 3J).

These observations reveal that transient medial and dorso-lateral epithelialized cell clusters may be the functional equivalents of the MHP and paired DLHPs of amniotes (and will be referred to henceforth as such), as they form at the right time and place to contribute to the formation of the neural groove (MHP), bending of the neuroectoderm and medial convergence of the neural folds (DLHPs).

Cell shape changes underlying DLHP and neural fold formation

To capture the dynamics of neural fold formation and image neuroectodermal cells at higher resolution, we mosaically expressed membrane-targeted GFP (mGFP) and imaged embryos at the 2-10 som stages in transverse sections (Figure 4). 3D reconstructions of some of these images were generated to gain a better understanding of the spatial relation between labeled cells and image cellular protrusions in multiple planes (Supplemental Figures 1, 2).

At 2 som, cells in the deep layer have a columnar shape with one end in contact with the basal lamina and a future apical surface oriented towards the midline (Figure 4A). These cells extend membrane protrusions into the superficial layer, which may promote radial intercalation (inset in Figure 4A).

191 At 5 som, cells in the dorso-lateral deep layer have undergone apical constriction and
192 basal expansion, forming DLHPs (yellow dotted circles and double arrowheads in Figure
193 4B,b1; Supplemental Figure 1). These cell shape changes may initiate the outpocketing of
194 the optic vesicles (ov in Figure 4B,b1). The bilaminar organization of the neural folds is
195 clearly visible at this stage. Neuroectoderm cells within the neural folds (arrows in Figure 3b1
196 and c1) are elongated and their basal poles are constricted, which gives them the
197 appearance of fanning out from a focal point (red circles in Figure 4b1 and c1) that spatially
198 coincides with a sharp bend in the neuroectoderm. The plasma membrane at the future
199 apical surface of these cells is ruffled, indicative of dynamic protrusive activity (Supplemental
200 Figure 2).

201 By 7 som (Figure 4D, Supplemental Figure 2), neuroectoderm cells of the neural folds
202 have elongated and reached the dorsal midline. They maintain their earlier organization with
203 basal poles constricted and clustered at a focal point on the basement membrane (red circle
204 in Figure 4d1). 3D reconstructions reveal that these cells are finger-shaped as they extend
205 across the dorsal midline. DLHP cells maintain their apical constriction/basal expansion and
206 further elongate, contributing to the expansion of the optic vesicles (dotted double arrowhead
207 in Figure 4d1).

208 At 10 som (Figure 4E, e1) deep cells in the eye field and neural folds have a columnar,
209 epithelial organization. Consistent with previous findings, eye field cells shorten along their
210 apico-basal axis by contracting their apical processes and coincidently transition to a more
211 dorso-ventral orientation [37] (dotted double arrow in Figure 4e1). Cuboidal non-neural
212 ectoderm cells cover the dorsal surface of the newly formed telencephalon (arrowheads in
213 Figure 4e1.

The dynamic cell shape changes in the deep layer of the neuroectoderm were quantified by measuring cell length and the apico:basal ratio of mGFP-labeled cells located at different positions along the medio-lateral axis of the ANP at 2, 5 and 7 som (Figure 5). These data reveal that the average length of DLHP cells increases while their apical:basal ratio decreases between 2 and 7 som, coincident with optic vesicle evagination. They also confirm that neuroectoderm cells of the neural folds elongate and adopt the reverse configuration, with basally constricted poles.

These findings indicate that zebrafish DLHP cells adopt a wedge shape similar to the cytoarchitecture of DLHPs in amphibians and amniotes, which enables epithelial bending. They further identify basal constriction of neuroectodermal cells in the neural folds as a cell shape change that contributes to neural fold formation.

MHP cells constrict apically and elongate

While mosaic expression of mGFP enabled high resolution imaging of DLHPs and neural folds, it resulted in few cells labeled in the medial superficial layer, where the MHP forms. Phalloidin labeling was therefore used to image these cells in 2 and 5 som embryos.

At the 2 som stage, some but not all medial/superficial cells immediately below the enveloping layer (EVL) are apically constricted, forming the MHP (Figure 6A-a2). By 5 som, MHP cells appear more densely packed, the majority of them are apically constricted and oriented towards the midline. Concomitant with these cell shape changes and the medial convergence of neural folds, MHP cells shift to a more ventral position (Figure 6B-b2. A small opening, the neural groove, is observed immediately above the MHP at this stage (NG in Figure 6b1).

Measurements of the apico:basal surface ratio of MHP cells in 5 som embryos confirmed that they are wedge-shaped (Figure 6c1). Similar to amphibians [41], apical constriction appears tightly coupled to cell elongation, as the length-to-width ratio (LWR) of MHP cells increases significantly between 2 and 5 som (Figure 6c2). Thus, both apical constriction and cell elongation appear to shape the MHP and contribute to tissue-level morphogenesis.

Another contributing factor to hingepoint formation in amniotes is the basal location of nuclei in both the medial and lateral hingepoints [42,43]. To evaluate the relative apico-basal position of DAPI-labeled nuclei in MHP cells, we measured the distance between the dorsal nuclear surface and the basal pole of MHP cells as a fraction of the total cell length (Figure 6c3). This analysis revealed that at 2 and 5 som stages the position of the nucleus does not change significantly and is therefore unlikely to contribute to wedging of this cell population.

Oscillatory constrictions progressively reduce the apical surface of MHP cells

To gain a better understanding of the dynamics of apical constriction and cell internalization, the ANP of embryos ubiquitously expressing mGFP was imaged from a dorsal view using time-lapse microscopy between 2 som to 4 som (n = 2 embryos, Figure 6D and Supplemental Figure 3). The focal plane was set immediately below the EVL, at the level of the MHP. These movies revealed clusters of medially-located cells that undergo progressive cell surface reduction (color-coded in Figure 6d1-d6), while the surface area of adjacent, more lateral cells remained unchanged for the duration of imaging (yellow asterisks in Figure 6d1-d6). EVL cells came into focus immediately posterior to the cells with reducing apices. Since the EVL is drawn inward as a result of its close contact with apically constricting MHP cells

(Figure 6B-b2), we surmise that apical constriction proceeds in a posterior-to-anterior direction. In later movie frames, EVL cells are no longer observed within the field of view, coinciding with the proximity of the neural folds to the midline (Supplemental Figure 3), indicating that the medial EVL cells eventually lose contact with the MHP and return to their original position, allowing the neural folds to fuse at the dorsal midline.

To further examine the dynamics of apical constriction, the surface area of superficial ANP cells was measured at regular intervals. Cells located at the midline (MHP cells, band width of 20 μm from the midline, Figure 7A, C) or immediately adjacent to the midline (MHP-adjacent cells, greater than 20 μm from the midline, Figure 7B) were scored. This analysis revealed that individual cells undergo pulsed contractions. Between pulses the surface area of cells expands slightly, but not back to original values (Figure 7A, C), resulting in a gradual decrease of pulsing amplitude over time, which is more pronounced for MHP cells than their immediate neighbors.

Together these data indicate that MHP cells undergo progressive narrowing of their apical pole via pulsed contractions and that these cellular dynamics proceed in a posterior-to-anterior direction.

Neural fold fusion is initiated at closure points and mediated by dynamic protrusive activity

In mice, neurulation proceeds unevenly along the anterior-posterior axis with multiple closure initiation sites [3], raising the question of whether neural fold fusion also occurs asynchronously in zebrafish. To address this, we performed time-lapse imaging of embryos mosaically expressing mGFP from a dorsal view around the time when opposing neural folds approach

the midline (n= 2 embryos, Figure 8A and Supplemental Figure 4). Neuroectoderm cells of the neural fold were identified based on their elongated shape and dorsal location (unlike MHP cells they do not become internalized).

These movies revealed that the neural folds have an arc shape with the apex positioned anteriorly (red asterisks in Figure 8A), which is strikingly similar to the expression domain of the telencephalon marker *emx3* at the onset of neural fold convergence (inset in Figure 8A). Neural fold fusion is initiated near the apex of the arch and proceeds in an anterior-to-posterior direction for a distance of approximately 35 µm (red dotted line in Figure 8a3). At this level, defined as closure point one (C1 in Figure 8a2), neural fold fusion proceeds asynchronously, as a second closure initiation site is formed more posteriorly (C2 in Figure 8A5), defining an eye-shaped opening (white dotted oval in Figure 6 a4, a5). A zippering process then begins at the anterior and posterior corners, progressing from both ends toward the middle (Figure a6,a7; Supplemental Figure 4).

The events that complete neural fold fusion in amniotes involve the extension of dynamic cellular projections towards the midline as opposing neural folds approach each other [17-19]. These cellular extensions are thought to function as transient bridges that promote the formation of stable intermediate closure points. Likewise, we observed that zebrafish neuroectodermal cells extend filopodia across the midline to establish contact with cells from the contralateral side. Furthermore, the cell bodies hyper-extend beyond the midline (Figure 6b3, b4 and Supplemental Figure 5), indicating that they interdigitate between neuroectoderm cells of the opposing neural fold. These cellular extensions are eventually retracted, clearing the midline, which coincides with the timing of epithelialization and the establishment of apical junctions (Figure 3D).

306 The presence of closure points and the usage of filopodia to establish contact with
307 neural fold cells across the midline reveal additional aspects of forebrain neurulation that are
308 conserved in zebrafish.
309
310 **Molecular characteristics of medial and lateral hingepoints**
311 Key features of cells that form hingepoints include apico-basal polarization, accumulation of
312 an apical contractile machinery composed of actin filaments (F-actin) and non-muscle myosin
313 II [44]. To test whether the MHP and DLHPs in the zebrafish forebrain have some or all of these
314 characteristics and to evaluate the timing of their maturation, the localization of Pard3-GFP (a
315 marker for apical polarity, transiently expressed following mRNA injection), F-actin
316 (phalloidin) and phospho-Myosin Light Chain II (anti-P-MLC) was examined in 3, 4 and 5 som
317 embryos (Figure 9).
318 Apical co-localization of Pard3-GFP and F-actin was confirmed in both the MHP and
319 DLHPs, beginning at the 3 som stage (data not shown) and became more prominent by 4
320 and 5 som (Figure 9A-F). Thus, while the establishment of apico-basal polarity is generally
321 delayed in the zebrafish neural plate relative to amniotes, the cell clusters that undergo apical
322 constriction in the ANP are epithelialized earlier than other neural plate cells, consistent with
323 previous observations [37]. P-MLC accumulation at the apical pole is slightly delayed relative to
324 Pad3-GFP, as it is only apparent by the 5 som stage in MHP cells where it overlaps with F-
325 actin (Figure 9J-L). In contrast, P-MLC enrichment is not observed in the DLHPs (open
326 arrowhead in Figure 9K). P-MLC also accumulates in the cell cortex of all neuroectoderm
327 cells where it overlaps with F-actin, in addition to the basal surface of EVL cells (arrow in
328 Figure 9H, K) and at the interface between the neuroectoderm and non-neural ectoderm

(dotted line in Figure 9J-L).

These findings reveal that both the MHP and DLHP undergo early epithelialization and accumulate F-actin at the apical cortex. However, the MHP and DLHPs are molecularly distinct structures given that the latter is not enriched for P-MLC.

Myosin contractility is required for MHP formation and neural fold convergence

During neural tube closure, the actomyosin cytoskeleton is thought to be a driving force for apical constriction [41]. To address a putative function for this molecular motor in mediating apical constriction in zebrafish, non-muscle myosin II (NMII) was blocked using blebbistatin and a translation-blocking morpholino (MO) targeting NMIIb [45] and the effect was analyzed in 5 som embryos. As expected, P-MLC levels were normal in blebbistatin-treated embryos (since this drug blocks NMII activity but not its phosphorylation) and reduced in NMIIB-MO injected embryos (Figure 10a1'', a2'', a3''). Both treatments severely disrupted apical constriction, resulting in absence of a clearly defined MHP and failure of these cells to elongate (Figure 10a1,a1' vs Figure 10a2, a2', a3, a3'). In contrast to superficial cells, cells in the deep layer retained their elongated shape (double arrowheads in Figure 10a1 versus a2,a3). Consistent with the earlier observation that the apices of DLHP cells do not accumulate P-MLC, these cells retained their wedge shape and apical F-actin accumulation in NMIIb MO-injected embryos (open arrowheads in Figure 10a3). These observations highlight the conserved function of actomyosin in driving apical constriction in hingepoint cells. The failure of MHP cells to elongate is unlikely due to the loss of cortical tension proposed by Rolo et al. (2009) [15] as P-MLC is present in both the superficial and deep layers of the ANP and rounded cells are restricted to the superficial layer. Another explanation is

that, as previously reported, apical constriction and microtubule-based cell elongation are orchestrated by the same effector proteins [41], and NMII may provide feedback information on the status of apical constriction in superficial cells.

At a morphological level, disruption of the actomyosin network causes neural tube defects that trace back to impaired apical constriction and convergent extension in *Xenopus* embryos [15]. To test whether myosin is similarly required for forebrain neural tube closure in zebrafish, control (untreated and DMSO-treated) and blebbistatin-treated embryos were labeled at the 2, 5 and 7 som stage via *in situ* hybridization using the telencephalon marker *emx3* (Figure 10B) and the width of the posterior-most emx3 domain was measured (Figure 10C). In contrast to control embryos, neural fold convergence was impaired in blebbistatin-treated embryos, beginning at the 5 som stage. It is possible that impaired convergent extension or expansion of the interface between the neuroectoderm and non-neural ectoderm layers of the neural folds contribute to this defect. However, failure of MHP cells to undergo apical constriction is likely to be a significant underlying cause given that disruption of several proteins implicated in this process, including Shroom3 [13] and GEF-H1, a RhoA-specific GEF [14] cause severe neural tube closure defects.

DISCUSSION

We report here on mechanisms of forebrain morphogenesis in the zebrafish embryo and reveal that this region of the brain is formed via a mode of primary neurulation, involving the use of hingepoints and neural folds.

The zebrafish MHP and paired DLHPs form in the superficial and deep layers of the eye field, respectively. The zebrafish MHP is more transient than its mammalian counterpart

since these cells eventually intercalate radially between deep layer cells, contributing to the expansion of the eye vesicle [37]. Hingepoints are restricted to the ANP in zebrafish, however they are also present in more posterior regions of the neural plate in amniotes. Despite this difference, individual cells in the medial zone of the hindbrain neural plate were recently shown to internalize via a myosin-dependent mechanism [46]. Such variation from the organized cell clusters forming hingepoints in the forebrain region of the zebrafish could be explained by the precocious epithelialization of the ANP [37]. It thus appears that there is a transition from clustered internalization mediated by the MHP in the forebrain to individual cell internalization in the hindbrain region.

A key feature of hingepoint cells is their reduced apical surface, which is in part due to actomyosin contractility [13,41,47,48]. Apical constriction is thought to function as a purse string to generate the force required to bring the neural folds together during cranial neurulation [49]. We provide evidence that the zebrafish MHP also utilizes an actomyosin-based contractile system. Assembly of this actomyosin network occurs via pulsed contractions with gradually decreasing amplitude, akin to the ratchet model first proposed in *Drosophila* and *C. elegans* [50-52] and later reported during neural tube closure in *Xenopus* [53]. We further show that disruption of myosin impairs neural fold convergence. These observations indicate that the actomyosin machinery is used across all vertebrate models of neurulation to drive cranial neural tube closure.

In contrast to the MHP, the paired DLHPs do not require myosin to apically constrict, suggesting that DLHP formation is regulated by a distinct mechanism. Consistent with this observation, McShane and colleagues report that cell packing at a dorso-ventral boundary in the mouse neural tube causes buckling of the neuroectoderm at the DLHPs [54]. It is possible

that such a mechanism also operates during zebrafish neurulation.

Neural folds in chick embryos form via a series of steps involving epithelial ridging, kinking, delamination and apposition [16], although the cellular basis of these morphogenetic events is not well understood. Elevation of the neural folds in the mouse cranial neural plate is dependent on expansion of the head mesenchyme [55]. Neural folds in the zebrafish are restricted to the ANP. The head mesenchyme is unlikely to play a significant mechanical role in neural fold elevation in zebrafish as the mesoderm layer immediately underlying the ANP is thin. We identify instead a neural fold-autonomous cell behavior, basal constriction, that may contribute to the early stages of neural fold elevation in zebrafish and possibly also in amniotes. Given that the neural folds converge medially, increasing the surface of apposition between the neuroectoderm and non-neural ectoderm, it is possible that basal constriction is transient and involves successive rows of neuroectodermal cells, akin to the epithelial rolling model described by Keller and Shook [56].

The final step of primary neurulation involves the convergence and fusion of the neural folds at the dorsal midline. Neural fold fusion is initiated at closure points in mammals and birds, however their timing and the order in which these points close varies across species[57]. We observe two closure points in the zebrafish forebrain that form an eye-shaped opening that narrows from the corners in a bidirectional manner. Fusion of the neural folds is mediated by the formation of dynamic, actin-rich cellular protrusions that span the midline and establish the first points of contact with neural fold cells from the contralateral side. Akin to mice [20,21], the cells that initiate contact between apposing neural folds in zebrafish derive from the neuroectoderm portion of the neural folds. The protrusive ends of the neuroectoderm cells interdigitate between their contralateral counterparts, forming a rod like

structure, the precursor of the telencephalon, which subsequently epithelializes. Once the neuroectoderm cells have met and fused, non-neural ectoderm cells complete their migration and fuse at the dorsal midline.

Together these findings have significant implications for our understanding of the evolution of neurulation and the relevance of this model organism to understand human neural tube development.

METHODS

Zebrafish strains/husbandry

Studies were performed using wildtype (AB) strains or *Tg(emx3:YFP)*^{b1200}[39] and embryos were raised at 28.5°C. All experiments were approved by the University of Maryland, Baltimore County's Institutional Animal Care and Use Committee (IACUC) and were performed according to national regulatory standards.

Nucleic acid and morpholino injections

Plasmids encoding membrane-targeted Green Fluorescent Protein (mGFP) (Richard Harland, University of California, Berkeley, CA, USA) and *pard3:egfp*[58] were linearized with NotI and transcribed using the SP6 mMESSAGE mMACHINE kit (Ambion, AM1340). For ubiquitous expression of mGFP or Par3d:eGFP, 50 pg of RNA was injected into 1-cell stage embryos. For mosaic expression of mGFP, 50 pg of RNA was injected into 1 or 2 of the four central blastomeres at the 16-cell stage. These blastomeres have a high probability for neural fate[59] and are easy to identify for reproducible injections.

MOs were designed and synthesized by GeneTools (Philomath, Oregon, USA) and injected into 1-cell stage embryos. *mhy10*(Non-muscle Myosin IIB, EXON2-intron2) was delivered at 3ng per injection.

mhy10: 5'-CTTCACAAATGTGGTCTTACCTTGA-3′ [45]

Microinjections were performed using a PCI-100 microinjector (Harvard Apparatus, Holliston, MA, USA).

Blebbistatin treatment

90% epiboly embryos were manually dechorionated in an agarose-covered petri dish with E3 medium. Once embryos reached the tailbud stage, they were placed into 50μM blebbistatin (B0560 Sigma-Aldrich) diluted with E3 and then incubated at 28.5°C. Stock solution of blebbistatin was prepared with DMSO as per manufacturer's instructions. Accordingly, a control group of embryos were treated with 1% DMSO diluted with E3 alongside every blebbistatin trial. Once the desired developmental stage was reached (2-, 5-, or 7-som), embryos were immediately fixed with 4% paraformaldehyde (PFA). As blebbistatin is light sensitive, embryos were kept in the dark as much as possible until fixation.

Fixed tissue preparations and immunolabeling

Embryos were fixed in 4% PFA for 16 hours at 4°C overnight. Immunolabeling was performed on whole mount embryos, which were then sectioned with a Vibratome (Vibratome 1500 sectioning system). Primary antibody incubation was performed for 48 hours at 4°C and secondary antibody incubation for 2.5 hours at room temperature.

Antibodies used: Rabbit anti-GFP at 1:1000 (Invitrogen, A11122), Rabbit anti-Sox3c at 1:2000 (Gift from Michael Klymkowsky), Rabbit anti-P-myosin light chain at 1:50 (Cell Signaling Technology, #3671S), and Mouse anti-p63 at 1:200 (Santa Cruz BioTechnology, SC-8431 no longer in production). Alexa Fluorophore secondary antibodies were all used at a 1:1000 concentration: Goat anti-Rabbit -488, -568, -594 and Goat anti-Mouse -488, -594.Alexa Fluor 488-conjugated or 594-conjugated Phalloidin (Invitrogen, A12379 and A12381) at 1:250 and DAPI (Invitrogen, D1306) were used according to manufacturer's instructions. Sections were mounted on glass slides using ProLong Diamond Antifade Mountant (Invitrogen, P36961). *Tg(emx3:YFP)*^{b1200}embryos were immunolabeled with anti-GFP to amplify the signal. mGFP and *pard3:eGFP*-injected embryos were not immunolabeled with anti-GFP.

Whole-mount *in situ*hybridization

In situ hybridization was performed as described [60]. *emx3* riboprobe template was generated by PCR amplification using cDNA from 24hpf embryos.

T7 promoter: **TAATACGACTCACTATAGGG**
emx3 antisense:
FWD: TCCATCCATCCTTCCCCCTT
RVS: **TAATACGACTCACTATAGGG**GTGCTGACTGCCTTTCCTCT

DIG-labeled riboprobes were generated using 2ul of PCR template with the Roche DIG RNA Labeling Kit (T7) (Sigma aldrich, SKU 11277073910)

Whole-mount imaging

Whole-mount imaging was carried out using a Zeiss Axioscope2 microscope. Embryos were imaged in a 2.5% glycerol solution.

Confocal microscopy

Time-lapse microscopy was performed as previously described [61]. Embryos were imaged using a Leica confocal microscope (Leica SP5 TCS 4D) at 15 sec/frame capturing <.5μm of tissue. All fluorescently labeled sections were imaged using a Leica confocal microscope (Leica SP5 TCS 4D).

Data Quantification

Medial-most-p63-positive-domain migration, Figure 3J: For each hemisphere of a tissue section, the distance between the medial-most p63 positive nucleus and the midline was manually scored. For each embryo, measurements were taken from tissue sections ranging along the anterior-posterior axis of the forebrain.

Deep layer cell morphology measurements, Figure 5: Cells were manually scored from non-projected z-stack images, where cellular outlines were visually determined from the mGFP signal. Cells were labeled as neuroectoderm neural fold cells based on the fan-like pattern of their basal projections in contact with the non-neural ectoderm. All other cells scored were within the morphologically distinct eye vesicle and were labeled as eye field cells. Neural ectoderm neural fold cells and eye field cells are not morphologically distinguishable at the 2 somitic stage and thus were not given cell type identities at that developmental stage.

Medial hinge cell morphology measurements, Figure 6C: Cells were manually scored from non-projected z-stack images of the overlay between the labeled actin cytoskeleton (phalloidin) and nucleus (DAPI, not shown in Figure 6) channels. Cellular outlines were visually determined from the phalloidin signal. For the nuclear position measurement (Fig 6c3), the distance from the dorsal edge of the nucleus to the basal membrane of the cell was scored and divided by the total cell length.

Cell ratcheting, Figure 7: Live movie z-stacks for the first 35 minutes (~2-4 somites, n=2) of each movie were max projected and cropped so the midline of the tissue horizontally bisected the image frame. The mGFP signal was then inverted and thresholded to produce a binary image. Measurements for individual cell surface areas were captured using the magic wand tool in ImageJ for every frame (15 seconds) until the cell left the field of view. Plotted on the x-axis is the order of frame measurements (frame 0, frame 1, frame 2,...) divided by the total number of frames for which that cell was scored to standardize between 0 and 1. Plotted on the y-axis, the initial value of each cell's surface area was subtracted from all measurements for that cell to initialize surface area's to zero. The data was binned (n=50) to obtain mean measurements and confidence intervals. Cells that underwent mitosis anytime during the movie were excluded. Cells were labeled as MHP if their surface area centroid from the first frame (t=0) was +- 20 μm from the midline with MHP-adjacent cells being labeled as such if their centroid was > +-20 μm from the midline.

emx3 in situ hybridization measurements, Figure 10C: The distance between the lateral edges of the posterior-most extent of the emx3 domain was manually scored for each embryo.

Statistical Analysis

The Mann-Whitney U test was used for all significance testing. The python function scipy.stats.mannwhitneyu(alternative='two-sided') was used to calculate the test statistic and P-value for each significance test. Graphs were generated using the python Seaborn package with the following functions: seaborn.boxplot(), seaborn.lmplot(), seaborn.violinplot(), seaborn.lineplot().

Data availability

The authors declare that all data supporting the findings of this study are available within the article and its supplementary information files or from the corresponding author upon reasonable request.

559 **REFERENCES**

560

561 1 Copp, A. J., Greene, N. D. & Murdoch, J. N. Dishevelled: linking convergent
562 extension with neural tube closure. *Trends Neurosci* **26**, 453-455,
563 doi:10.1016/S0166-2236(03)00212-1 (2003).
564 2 Keller, R. Shaping the vertebrate body plan by polarized embryonic cell
565 movements. *Science* **298**, 1950-1954, doi:10.1126/science.1079478 (2002).
566 3 Copp, A. J., Greene, N. D. & Murdoch, J. N. The genetic basis of mammalian
567 neurulation. *Nat Rev Genet* **4**, 784-793, doi:10.1038/nrg1181 (2003).
568 4 Morriss-Kay, G. M. Growth and development of pattern in the cranial neural
569 epithelium of rat embryos during neurulation. *J Embryol Exp Morphol* **65 Suppl**,
570 225-241 (1981).
571 5 Baker, P. C. & Schroeder, T. E. Cytoplasmic filaments and morphogenetic
572 movement in the amphibian neural tube. *Dev Biol* **15**, 432-450 (1967).
573 6 Sadler, T. W., Greenberg, D., Coughlin, P. & Lessard, J. L. Actin distribution
574 patterns in the mouse neural tube during neurulation. *Science* **215**, 172-174,
575 doi:10.1126/science.7031898 (1982).
576 7 Morriss-Kay, G. & Tuckett, F. The role of microfilaments in cranial neurulation in
577 rat embryos: effects of short-term exposure to cytochalasin D. *J Embryol Exp*
578 *Morphol* **88**, 333-348 (1985).
579 8 Schoenwolf, G. C., Folsom, D. & Moe, A. A reexamination of the role of
580 microfilaments in neurulation in the chick embryo. *Anat Rec* **220**, 87-102,
581 doi:10.1002/ar.1092200111 (1988).
582 9 Ybot-Gonzalez, P. & Copp, A. J. Bending of the neural plate during mouse
583 spinal neurulation is independent of actin microfilaments. *Dev Dyn* **215**, 273-
584 283, doi:10.1002/(SICI)1097-0177(199907)215:3<273::AID-AJA9>3.0.CO;2-H
585 (1999).
586 10 Kinoshita, N., Sasai, N., Misaki, K. & Yonemura, S. Apical accumulation of Rho
587 in the neural plate is important for neural plate cell shape change and neural
588 tube formation. *Mol Biol Cell* **19**, 2289-2299, doi:10.1091/mbc.E07-12-1286
589 (2008).
590 11 Hildebrand, J. D. & Soriano, P. Shroom, a PDZ domain-containing actin-binding
591 protein, is required for neural tube morphogenesis in mice. *Cell* **99**, 485-497
592 (1999).
593 12 Xu, W., Baribault, H. & Adamson, E. D. Vinculin knockout results in heart and
594 brain defects during embryonic development. *Development* **125**, 327-337
595 (1998).
596 13 Haigo, S. L., Hildebrand, J. D., Harland, R. M. & Wallingford, J. B. Shroom
597 induces apical constriction and is required for hingepoint formation during
598 neural tube closure. *Curr Biol* **13**, 2125-2137 (2003).
599 14 Itoh, K., Ossipova, O. & Sokol, S. Y. GEF-H1 functions in apical constriction
600 and cell intercalations and is essential for vertebrate neural tube closure. *J Cell*
601 *Sci* **127**, 2542-2553, doi:10.1242/jcs.146811 (2014).

15 Rolo, A., Skoglund, P. & Keller, R. Morphogenetic movements driving neural tube closure in Xenopus require myosin IIB. *Dev Biol* **327**, 327-338, doi:10.1016/j.ydbio.2008.12.009 (2009).

16 Lawson, A., Anderson, H. & Schoenwolf, G. C. Cellular mechanisms of neural fold formation and morphogenesis in the chick embryo. *Anat Rec* **262**, 153-168, doi:10.1002/1097-0185(20010201)262:2<153::AID-AR1021>3.0.CO;2-W (2001).

17 Pyrgaki, C., Trainor, P., Hadjantonakis, A. K. & Niswander, L. Dynamic imaging of mammalian neural tube closure. *Dev Biol* **344**, 941-947, doi:10.1016/j.ydbio.2010.06.010 (2010).

18 Ray, H. J. & Niswander, L. A. Dynamic behaviors of the non-neural ectoderm during mammalian cranial neural tube closure. *Dev Biol* **416**, 279-285, doi:10.1016/j.ydbio.2016.06.030 (2016).

19 Rolo, A. *et al.* Regulation of cell protrusions by small GTPases during fusion of the neural folds. *Elife* **5**, e13273, doi:10.7554/eLife.13273 (2016).

20 Geelen, J. A. & Langman, J. Closure of the neural tube in the cephalic region of the mouse embryo. *Anat Rec* **189**, 625-640, doi:10.1002/ar.1091890407 (1977).

21 Geelen, J. A. & Langman, J. Ultrastructural observations on closure of the neural tube in the mouse. *Anat Embryol (Berl)* **156**, 73-88 (1979).

22 Massarwa, R., Ray, H. J. & Niswander, L. Morphogenetic movements in the neural plate and neural tube: mouse. *Wiley Interdiscip Rev Dev Biol* **3**, 59-68, doi:10.1002/wdev.120 (2014).

23 Waterman, R. E. Topographical changes along the neural fold associated with neurulation in the hamster and mouse. *Am J Anat* **146**, 151-171, doi:10.1002/aja.1001460204 (1976).

24 Criley, B. B. Analysis of embryonic sources and mechanims of development of posterior levels of chick neural tubes. *J Morphol* **128**, 465-501, doi:10.1002/jmor.1051280406 (1969).

25 Griffith, C. M., Wiley, M. J. & Sanders, E. J. The vertebrate tail bud: three germ layers from one tissue. *Anat Embryol (Berl)* **185**, 101-113 (1992).

26 Lowery, L. A. & Sive, H. Strategies of vertebrate neurulation and a re-evaluation of teleost neural tube formation. *Mech Dev* **121**, 1189-1197, doi:10.1016/j.mod.2004.04.022 (2004).

27 Andres Collazo, J. A. B., and Ray Keller. A Phylogenetic Perspective on Teleost Gastrulation. *The American Naturalist* **144**, 133-152 (1994).

28 Kimmel, C. B., Ballard, W. W., Kimmel, S. R., Ullmann, B. & Schilling, T. F. Stages of embryonic development of the zebrafish. *Dev Dyn* **203**, 253-310, doi:10.1002/aja.1002030302 (1995).

29 Papan, C. & Campos-Ortega, J. A. On the formation of the neural keel and neural tube in the zebrafishDanio (Brachydanio) rerio. *Roux Arch Dev Biol* **203**, 178-186, doi:10.1007/BF00636333 (1994).

30 Hong, E. & Brewster, R. N-cadherin is required for the polarized cell behaviors that drive neurulation in the zebrafish. *Development* **133**, 3895-3905, doi:10.1242/dev.02560 (2006).

31 Strahle, U. & Blader, P. Early neurogenesis in the zebrafish embryo. *FASEB J* **8**, 692-698, doi:10.1096/fasebj.8.10.8050667 (1994).

32 Reichenbach, A., Schaaf, P. & Schneider, H. Primary neurulation in teleosts--evidence for epithelial genesis of central nervous tissue as in other vertebrates. *J Hirnforsch* **31**, 153-158 (1990).

33 Miyayama, Y. & Fujimoto, T. Fine morphological study of neural tube formation in the teleost, Oryzias latipes. *Okajimas Folia Anat Jpn* **54**, 97-120 (1977).

34 Schmidt, R., Strahle, U. & Scholpp, S. Neurogenesis in zebrafish - from embryo to adult. *Neural Dev* **8**, 3, doi:10.1186/1749-8104-8-3 (2013).

35 Cearns, M. D., Escuin, S., Alexandre, P., Greene, N. D. & Copp, A. J. Microtubules, polarity and vertebrate neural tube morphogenesis. *J Anat* **229**, 63-74, doi:10.1111/joa.12468 (2016).

36 Yamaguchi, Y. & Miura, M. How to form and close the brain: insight into the mechanism of cranial neural tube closure in mammals. *Cell Mol Life Sci* **70**, 3171-3186, doi:10.1007/s00018-012-1227-7 (2013).

37 Ivanovitch, K., Cavodeassi, F. & Wilson, S. W. Precocious acquisition of neuroepithelial character in the eye field underlies the onset of eye morphogenesis. *Dev Cell* **27**, 293-305, doi:10.1016/j.devcel.2013.09.023 (2013).

38 England, S. J., Blanchard, G. B., Mahadevan, L. & Adams, R. J. A dynamic fate map of the forebrain shows how vertebrate eyes form and explains two causes of cyclopia. *Development* **133**, 4613-4617, doi:10.1242/dev.02678 (2006).

39 Viktorin, G., Chiuchitu, C., Rissler, M., Varga, Z. M. & Westerfield, M. Emx3 is required for the differentiation of dorsal telencephalic neurons. *Dev Dyn* **238**, 1984-1998, doi:10.1002/dvdy.22031 (2009).

40 Schroeder, T. E. Neurulation in Xenopus laevis. An analysis and model based upon light and electron microscopy. *J Embryol Exp Morphol* **23**, 427-462 (1970).

41 Suzuki, M., Morita, H. & Ueno, N. Molecular mechanisms of cell shape changes that contribute to vertebrate neural tube closure. *Dev Growth Differ* **54**, 266-276, doi:10.1111/j.1440-169X.2012.01346.x (2012).

42 Smith, J. L. & Schoenwolf, G. C. Cell cycle and neuroepithelial cell shape during bending of the chick neural plate. *Anat Rec* **218**, 196-206, doi:10.1002/ar.1092180215 (1987).

43 Smith, J. L. & Schoenwolf, G. C. Role of cell-cycle in regulating neuroepithelial cell shape during bending of the chick neural plate. *Cell Tissue Res* **252**, 491-500 (1988).

44 Lee, J. Y. & Harland, R. M. Endocytosis is required for efficient apical constriction during Xenopus gastrulation. *Curr Biol* **20**, 253-258, doi:10.1016/j.cub.2009.12.021 (2010).

45 Gutzman, J. H., Sahu, S. U. & Kwas, C. Non-muscle myosin IIA and IIB differentially regulate cell shape changes during zebrafish brain morphogenesis. *Dev Biol* **397**, 103-115, doi:10.1016/j.ydbio.2014.10.017 (2015).

46 Araya, C. *et al.* Cdh2 coordinates Myosin-II dependent internalisation of the zebrafish neural plate. *Sci Rep* **9**, 1835, doi:10.1038/s41598-018-38455-w (2019).

47 Karfunkel, P. The activity of microtubules and microfilaments in neurulation in the chick. *J Exp Zool* **181**, 289-301, doi:10.1002/jez.1401810302 (1972).

48 Lee, C., Scherr, H. M. & Wallingford, J. B. Shroom family proteins regulate gamma-tubulin distribution and microtubule architecture during epithelial cell shape change. *Development* **134**, 1431-1441, doi:10.1242/dev.02828 (2007).

49 Sawyer, J. M. *et al.* Apical constriction: a cell shape change that can drive morphogenesis. *Dev Biol* **341**, 5-19, doi:10.1016/j.ydbio.2009.09.009 (2010).

50 Martin, A. C., Kaschube, M. & Wieschaus, E. F. Pulsed contractions of an actin-myosin network drive apical constriction. *Nature* **457**, 495-499, doi:10.1038/nature07522 (2009).

51 Martin, A. C. & Goldstein, B. Apical constriction: themes and variations on a cellular mechanism driving morphogenesis. *Development* **141**, 1987-1998, doi:10.1242/dev.102228 (2014).

52 Solon, J., Kaya-Copur, A., Colombelli, J. & Brunner, D. Pulsed forces timed by a ratchet-like mechanism drive directed tissue movement during dorsal closure. *Cell* **137**, 1331-1342, doi:10.1016/j.cell.2009.03.050 (2009).

53 Suzuki, M. *et al.* Distinct intracellular Ca(2+) dynamics regulate apical constriction and differentially contribute to neural tube closure. *Development* **144**, 1307-1316, doi:10.1242/dev.141952 (2017).

54 McShane, S. G. *et al.* Cellular basis of neuroepithelial bending during mouse spinal neural tube closure. *Dev Biol* **404**, 113-124, doi:10.1016/j.ydbio.2015.06.003 (2015).

55 Zohn, I. E., Anderson, K. V. & Niswander, L. The Hectd1 ubiquitin ligase is required for development of the head mesenchyme and neural tube closure. *Dev Biol* **306**, 208-221, doi:10.1016/j.ydbio.2007.03.018 (2007).

56 Keller, R. & Shook, D. The bending of cell sheets--from folding to rolling. *BMC Biol* **9**, 90, doi:10.1186/1741-7007-9-90 (2011).

57 Nikolopoulou, E., Galea, G. L., Rolo, A., Greene, N. D. & Copp, A. J. Neural tube closure: cellular, molecular and biomechanical mechanisms. *Development* **144**, 552-566, doi:10.1242/dev.145904 (2017).

58 von Trotha, J.W., Campos-Ortega, J.A., Reugels, A.M. Apical localization of ASIP/PAR-3:EGFP in zebrafish neuroepithelial cells involves the oligomerization domain CR1, the PDZ domains, and the C-terminal portion of the protein. *Dev Dyn* **235,** 967-77 (2006).

59 Strehlow, D., Heinrich, G. & Gilbert, W. The fates of the blastomeres of the 16-cell zebrafish embryo. *Development* **120**, 1791-1798 (1994).

60 Thisse, C., Thisse, B., Schilling, T. F. & Postlethwait, J. H. Structure of the zebrafish snail1 gene and its expression in wild-type, spadetail and no tail mutant embryos. *Development* **119**, 1203-1215 (1993).

61 Jayachandran, P., Hong, E. & Brewster, R. Labeling and imaging cells in the zebrafish hindbrain. *J Vis Exp*, doi:10.3791/1976 (2010).

ACKNOWLEDGEMENTS

Funds from Howard Hughes Medical Institute through the UMBC Precollege and Undergraduate Science Education Program supported J. Werner and D. Brooks. Funds from NIH/NIGMS grants # T32-GM055036 and # R25-GM066706 and NSF LSAMP BD grant # 1500511 to UMBC supported M. Negesse. Funds from NSF LSAMP grant # 1619676 to UMBC supported J. Johnson. Funds from NIH/NIGMS MARCU*STAR T34 grant # HHS 00026 to UMBC supported D. Brooks and A. Caldwell. We thank the following people for their contributions: Tagide deCarvalho for her help with confocal imaging and image processing; Corinne Houart for the *Tg(emx3:YFP)*^{b1200} transgenic line; Jennifer Gutzman for the gift of *myh10* morpholino and Mark Van Doren for his comments on the manuscript.

AUTHOR CONTRIBUTIONS

J.W. designed and performed all experiments and carried out data analysis. M.N. identified neural fold closure points, annotated movie files and generated illustrations. D.B. and A.C. contributed to the experiments and analysis of cell polarity and myosin function. J.J. contributed to the analysis of myosin function. R.B. oversaw experimental design and analysis and wrote the manuscript.

COMPETING INTERESTS

766 The authors declare no competing interests

767

768 **MATERIALS AND CORRESPONDENCE**

769 Rachel Brewster

770

FIGURES

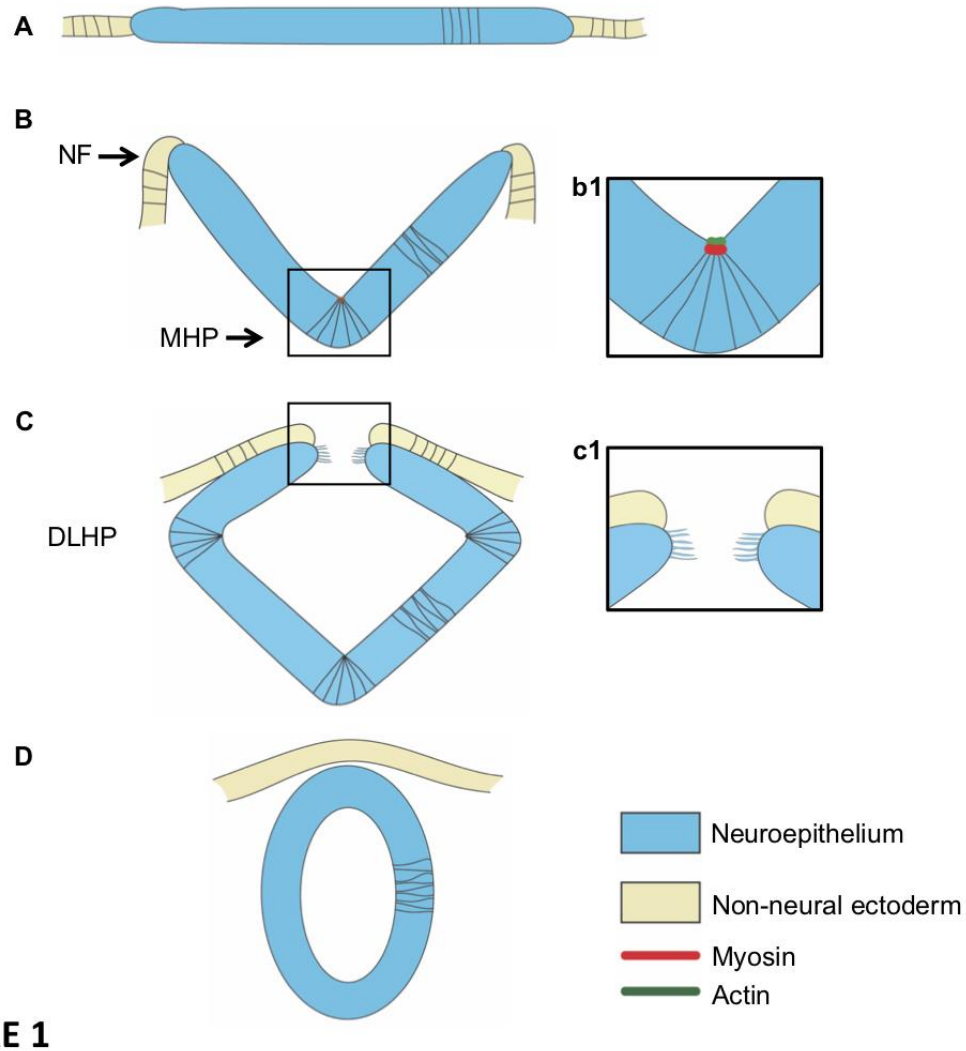

FIGURE 1

Figure 1. Neurulation in amniotes. Cross sectional illustration of stages of neurulation in amniotes. (A) The neural plate and adjacent non neural ectoderm. (B) Medial hingepoint formation shapes the neural groove and elevates the neural folds. (b1) Illustration of medial hingepoint cells that are apically-constricted and enriched for actomyosin at their apex. (C) Dorso-lateral hingepoint formation brings the neural folds in close apposition. (c1) Filopodial extensions establish contact between neural fold cells across the midline. In the mouse forebrain the first contact is established between neuroectodermal cells. (D) The neural folds fuse medially, separating the epidermis from the neural tube. Abbreviations: DLHP = dorso-lateral hingepoint; MHP = medial hingepoint; NF = neural fold.

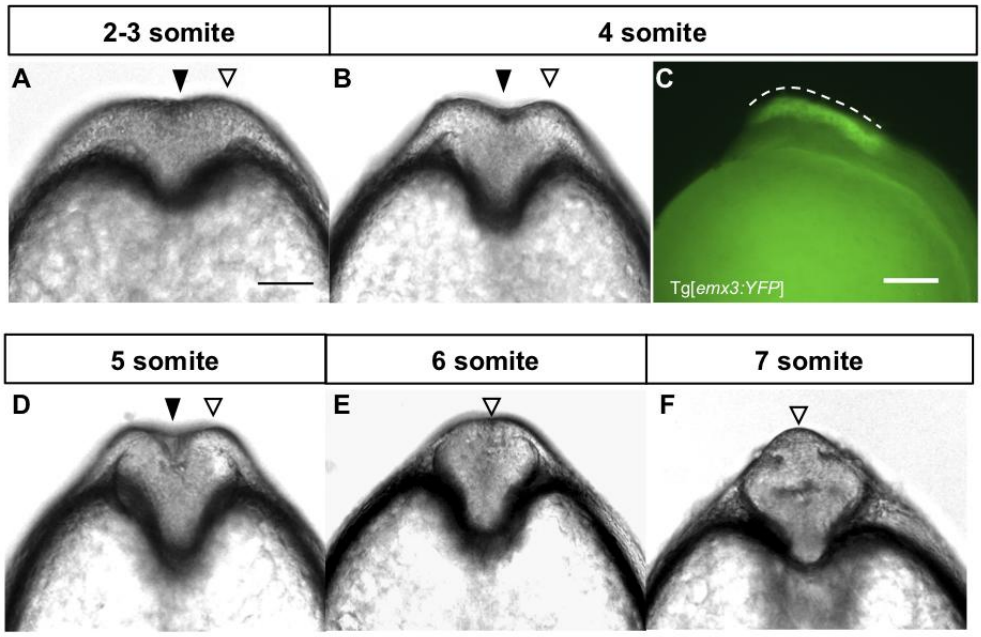

Figure 2. Presence of a neural groove and neural fold-like structures in the zebrafish forebrain. (A, B, D-F) Optical sections at the level of the forebrain of WT embryos at the 2-3 som (A), 4 som (B), 5 som (D), 6 som (E) and 7 som (F) stages. (C) Side view of a 4 som Tg[*emx3:YFP)* embryo. Annotations: black arrowhead = median groove, white open arrowhead = elevated neural-fold-like structure, dotted line = A-P range of the neural folds. Scale bars in A and C: 100 µm.

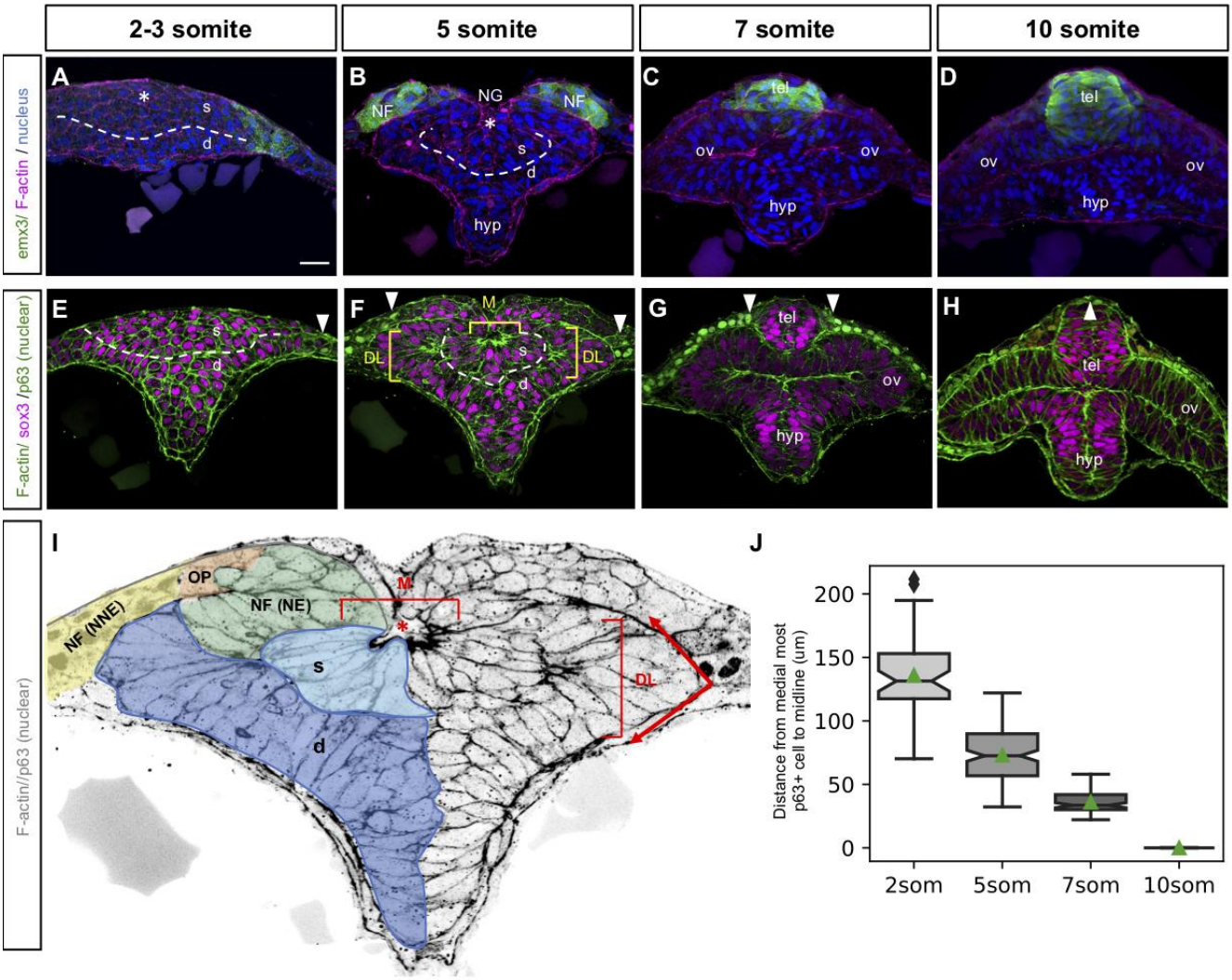

Figure 3. Hingepoints and neural folds contribute to forebrain morphogenesis. (A-D). Transverse sections through the ANP/prospective forebrain of 2-3 som (A, E), 5 som (B, F), 7 som (C, G) and 10 som (D, H) embryos. (A-D) Tg[*emx3:YFP*] embryos labeled with anti-GFP (green), phalloidin (F-actin, magenta) and DAPI (nuclei, blue). (E-H) WT embryos labeled with phalloidin (F-actin, green), anti-Sox3 (magenta) and anti-p63 (nuclear label, green). (I) Higher magnification image of panel F, grey scaled to reveal F-actin and p63 and pseudo-colored on the left side according to cell identity - color code: light blue: superficial eye field cells, dark blue: deep eye field cells that apically constrict to form the optic vesicles, green: neural component of the neural fold, orange: olfactory placode (cells that are Sox3/p63-negative), yellow: non-neural component of the neural fold. (J) Measurement of neural fold convergence, scored as the distance between the medial-most p63-positive cells on either side of the midline at different developmental stages. 2 som: 48 measurements across 14 embryos; 5 som: 144 measurements across 16 embryos; 7 som: 87 measurements across 10 embryos; 10 som: p63 domain is fused, no measurements. Statistical analysis: Mann-Whitney U tests, two-sided; 2 som vs 5 som : P = 1.18e^-21; 2 som vs 7 som : P = 8.35e^-22; 5 som vs 7 som : P = 2.14e^-31. Abbreviations: d = deep layer; DLHP = Dorso-lateral hingepoints; hyp = hypothalamus; MHP = Medial hingepoint; ov = optic vesicle; s = superficial layer; tel = telencephalon. Annotations: double white arrow = placodal cells; white arrowhead = medial-most epidermis; red asterisk = neuropore. All Scale bars: 25 μm.

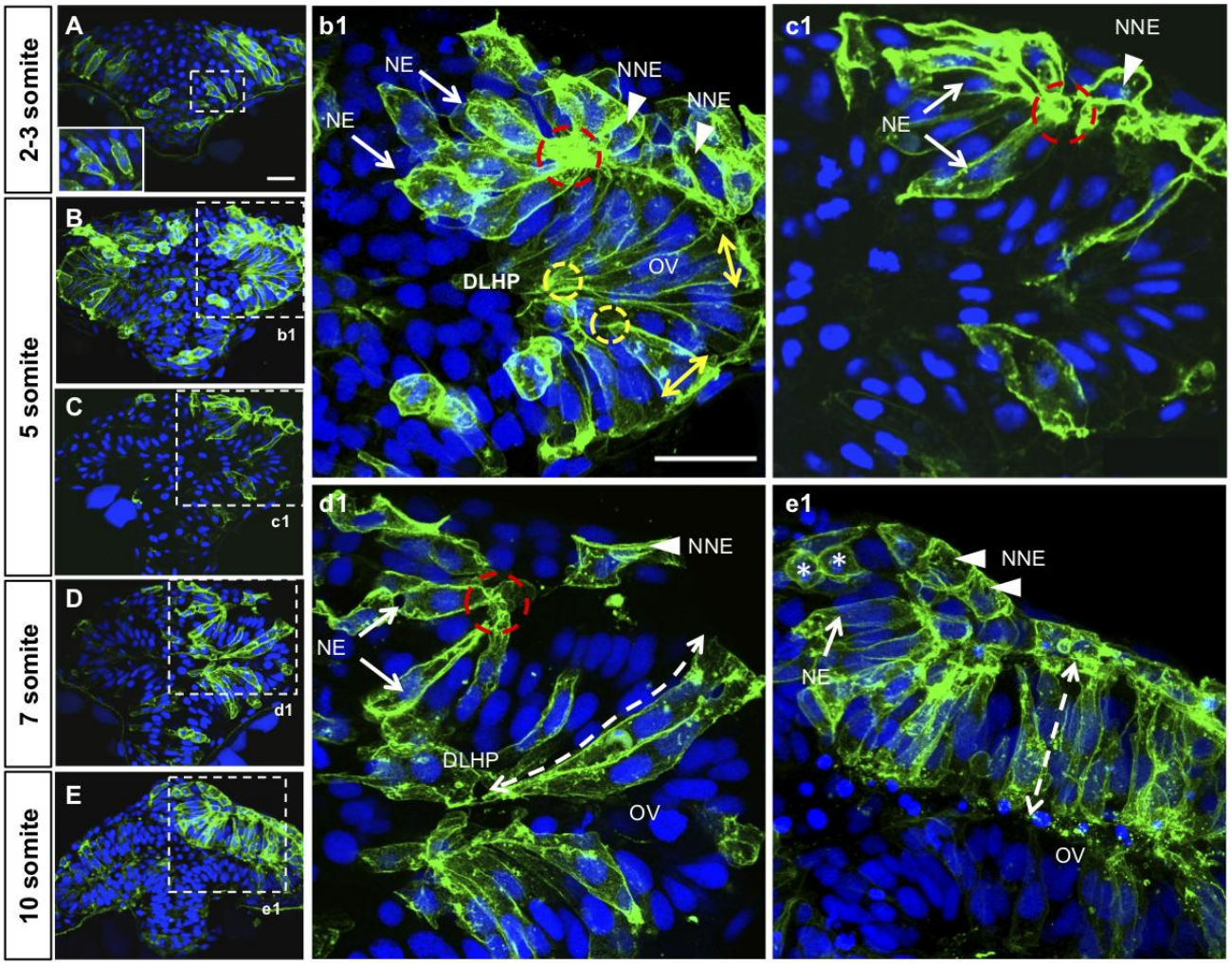

Figure 4. Cell shape changes in the deep layer of the ANP that contribute to DLHP and neural fold formation. (A-E) Transverse section, at the level of the forebrain, of embryos at the 2-3 (A), 5 (B, b1, C, c1), 7 (D, d1) and 10 (E, e1) somite stages mosaically-expressing mGFP (green) and labeled with the nuclear marker DAPI (blue). The inset in A is a higher magnification of dashed area in A**.** (b1-e1) Higher magnifications of regions delineated by dotted lines in (A-E). Annotations: red dashed circle = basal constriction of NE component of neural fold; yellow circle = apical constriction of DLHP cells; arrows = NE component of neural fold; arrowheads = NNE component of neural folds; double dashed arrow = elongated deep cells of the optic vesicle, asterisks = dividing cells in the prospective telencephalon. Scale bars: 25 μm in A and b1.

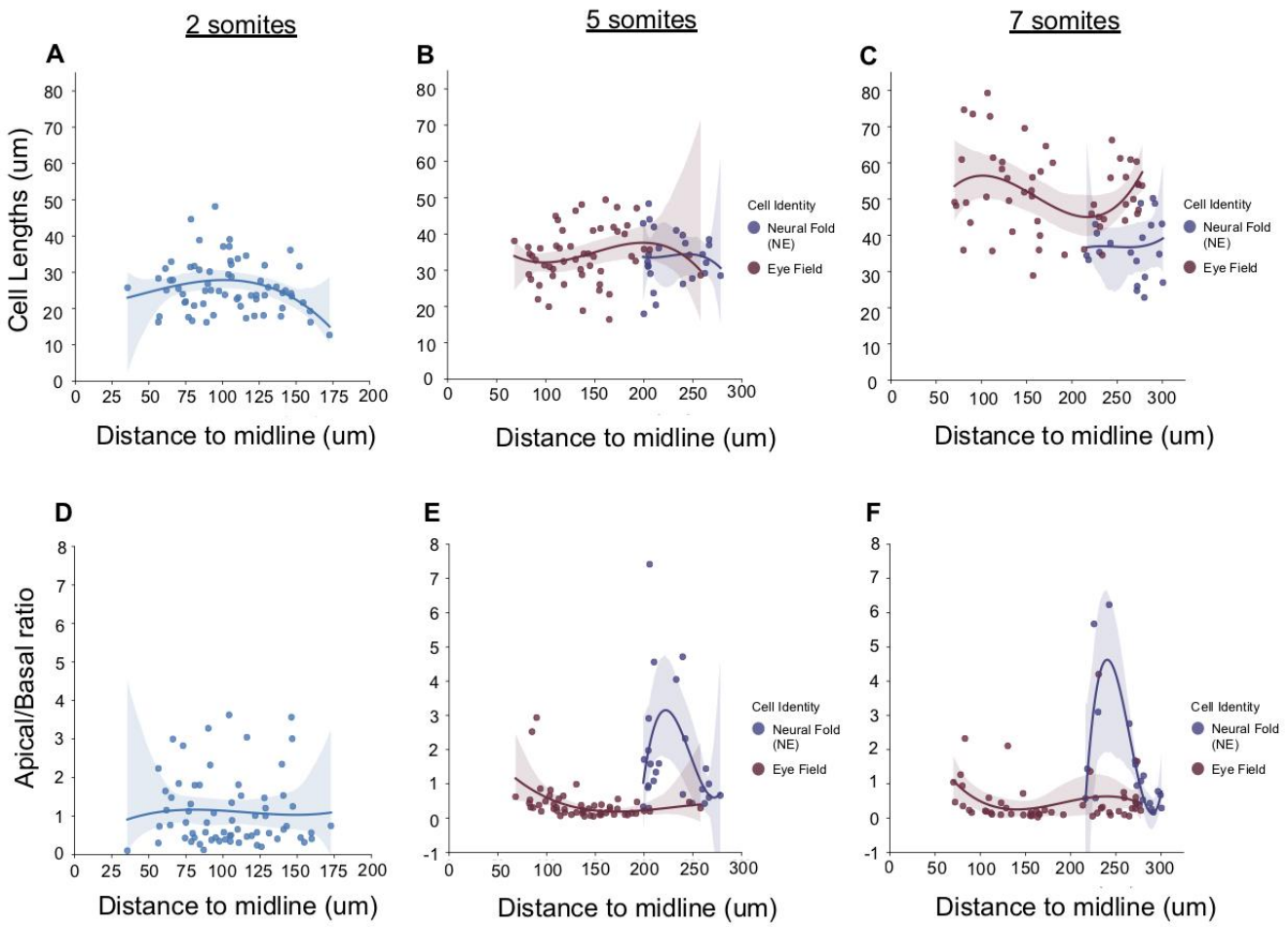

Figure 5. Measurements of cell shape changes in the deep neuroectodermal layer and neural folds. (A-C) Measurements of cell lengths (μM, Y axis) of m-GFP-labeled cells at different positions relative to the ANP midline (μM, X axis). Measurements begin in the region fated to become the optic vesicles. (D-F) Measurements of the apico:basal surface ratio of m-GFP-labeled cells at different positions relative to the ANP midline (μM, X axis). Measurements begin in the region fated to form the optic vesicles. The original scatter plot was fitted to a 3rd degree polynomial. Confidence intervals for the polynomial are 95% and were calculated with 1000 bootstraps. Color code: blue = neuroectodermal cells of the deep layer of 2 som stage embryos that are not yet identifiable based on cellular morphology; red = cells that form the optic vesicles; blue = cells that form the neuroectodermal component of the neural folds.

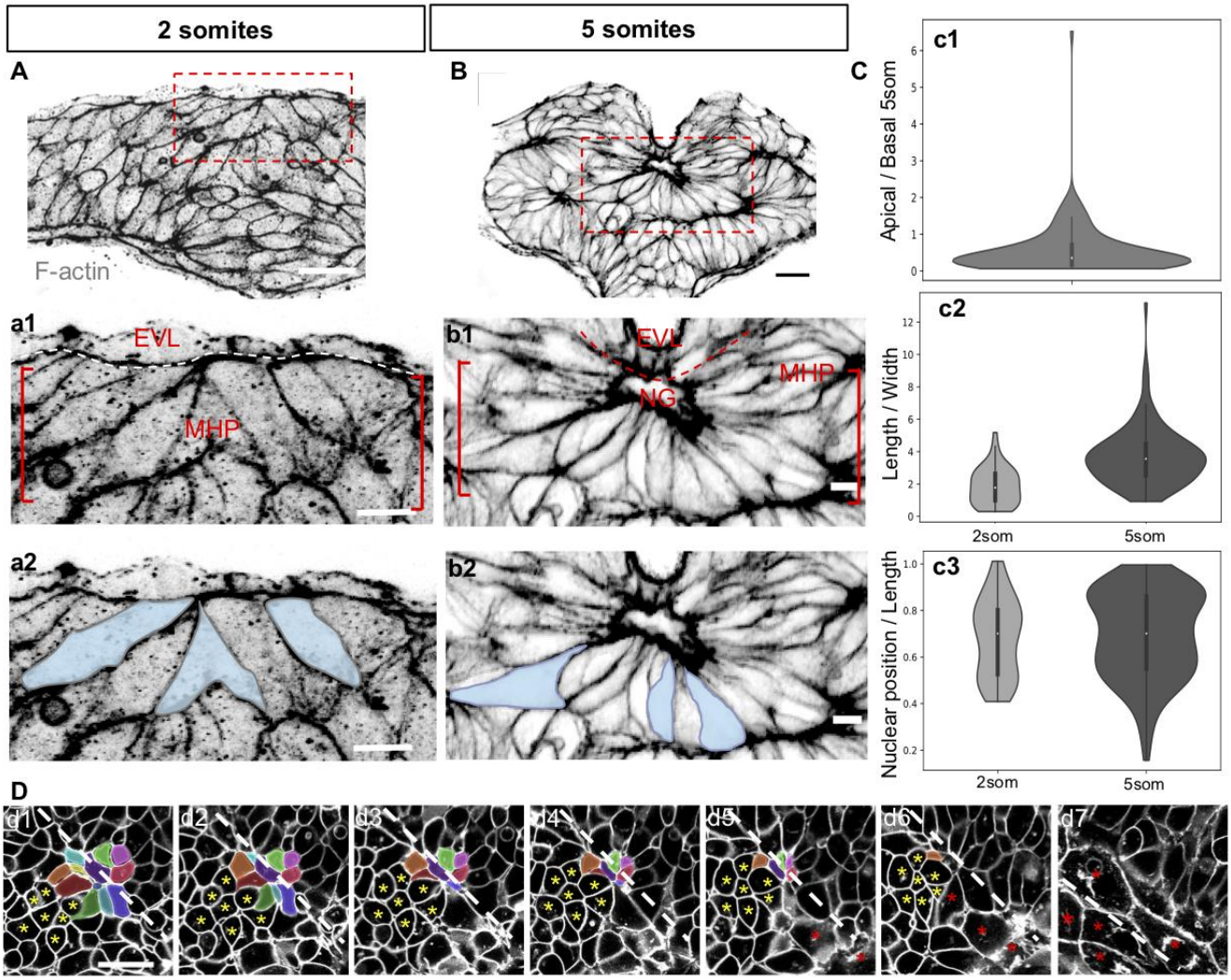

Figure 6. Apical constriction of MHP cells. (A-b2) Transverse sections through the ANP at the 2 (A, a1, a2) and 5 (B, b1, b2) som stages labeled with phalloidin (shown in greyscale). (a1-b2) are higher magnifications of the boxed areas in A and B, revealing the organization of the medial ANP (a1, b1) and the shape of individual MHP cells pseudo-colored in blue (a2, b2). (C) Quantitation of cell shape changes. (c1) Measurements of apical:basal surface ratio. (c2) Measurement of length-to-width (LWR) ratio at 2 som (n= 47 cells from 5 embryos) and 5 som (n= 115 cells from 4 embryos). A Mann-Whitney two-sided U Test revealed that the LWR increase between 2 som and 5 som is statistically significant (P = 7.80e^-11). (c3) Relative position of nucleus at 2 and 5 som measured in the same cell population (c3). Mean nuclear position/cell length of .682 ± .0240 at 2 som vs .696 ± .0174 at 5 som is not statistically significant using a Mann Whitney U test (P= .419). (E) Still frames of time lapse movie of m-GFP labeled embryo imaged from a dorsal view. Individual MHP cells are pseudo-colored, A cluster of cells adjacent to the MHP is indicated with yellow asterisks and EVL cells are labeled with red asterisks . Abbreviations: EVL = enveloping layer; MHP = medial hingepoint; NG = neural groove. Annotations: asterisk = medial groove; brackets = MHP region. Scale bars: 25 μm in A and B, 10 μm in a1, a2, b1, b2, d1.

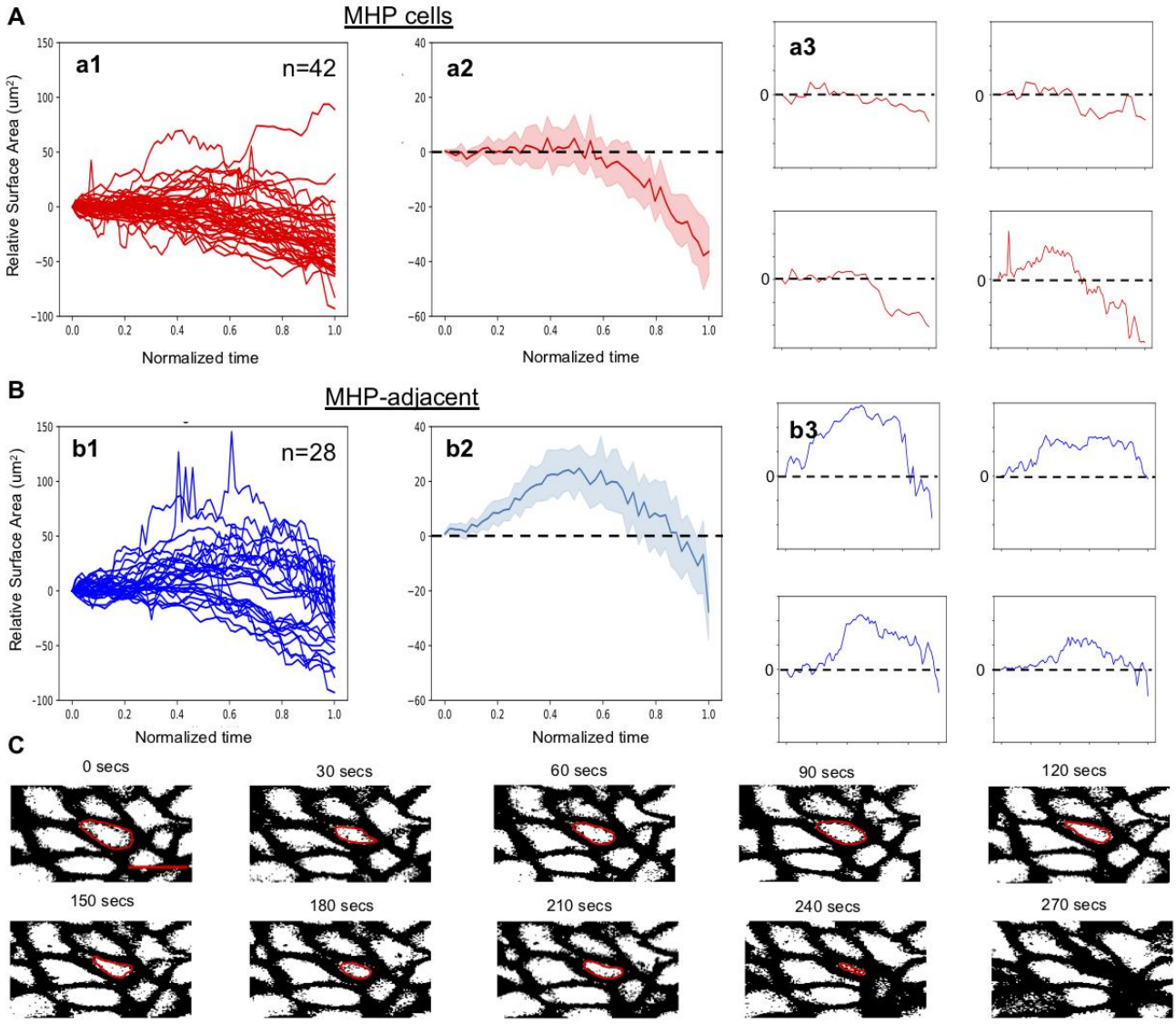

Figure 7. Oscillatory constriction with decreasing amplitude reduces the apical surface of MHP cells. (A) Measurements of medial, MHP cells. (a1) Relative apical surface areas over time for individual MHP cells. (a2) Mean values of MHP relative apical surface areas over time, 95% confidence interval. (a3) Representative traces of relative apical surface areas over time for individual MHP cells**.** (B) Measurements of MHP-adjacent cells. (b1) Relative apical surface areas over time for individual MHP-adjacent cells. (b2) Mean values of MHP-adjacent relative apical surface areas over time, 95% confidence interval. (a3) Representative traces of relative apical surface areas over time for individual MHP-adjacent cells. (C) Still frames of time-lapse movie of m-GFP labeled cells shown in grey-scale. The oscillatory behavior of one cell, outlined in red, is shown over time. Scale bar: 10 μm in c1.

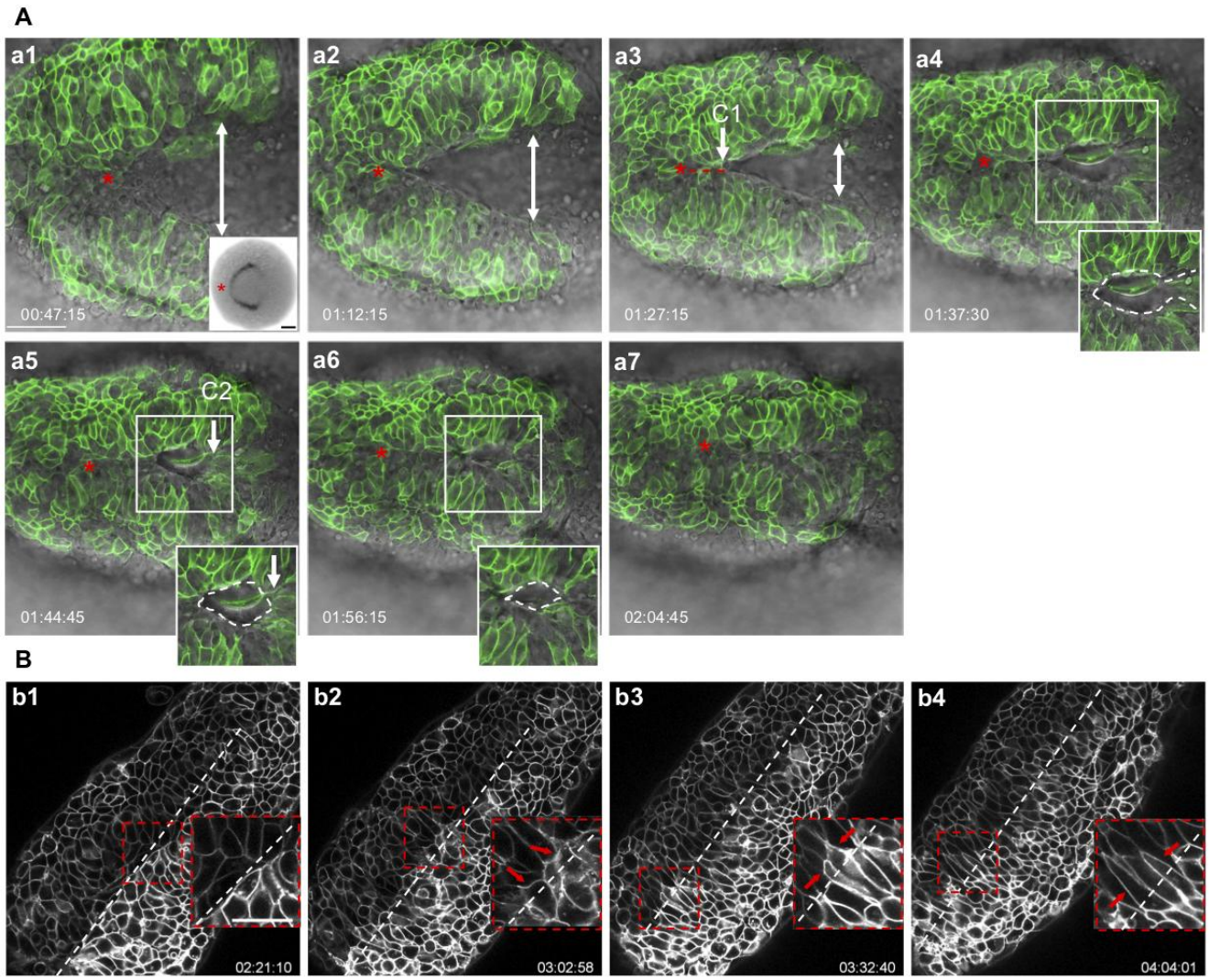

Figure 8. Dynamics of neural fold fusion. (A, a1-a7) Time lapse movie frames of an embryo expressing mosaic GFP, imaged from a dorsal view, showing the initiation of neural tube closure. Images are overlays of the green and brightfield channels. Inset in a1 shows a dorsal view of an *emx3*-labeled embryo. Insets in a4-a6 outline the eye-shaped opening that forms between closure sites one (CP1) and two (CP2) (B) Grey-scale time-lapse movie frames of an mGFP-labeled embryo imaged from a dorsal view, revealing the final stages of neural fold fusion. Insets in the lower right corner of panels b1-b4 are higher magnification views of boxed areas. Abbreviations: C1, C2: closure sites one and two. Annotations: red asterisk: apex of the neural fold arc; red dotted line: synchronous and posteriorly-directed neural fold fusion anterior to closure point one; white double arrows: distance between the neural folds; white dotted oval: eye shaped opening, the corners of which are defined by closure points one and two; white dotted line: embryonic midline; red arrows: filopodia extending across the midline; time-elapse is shown at the bottom of each panel.Scale bars: 50 μm in a1, 100 μm in a1 inset, and 25 μm in b1.

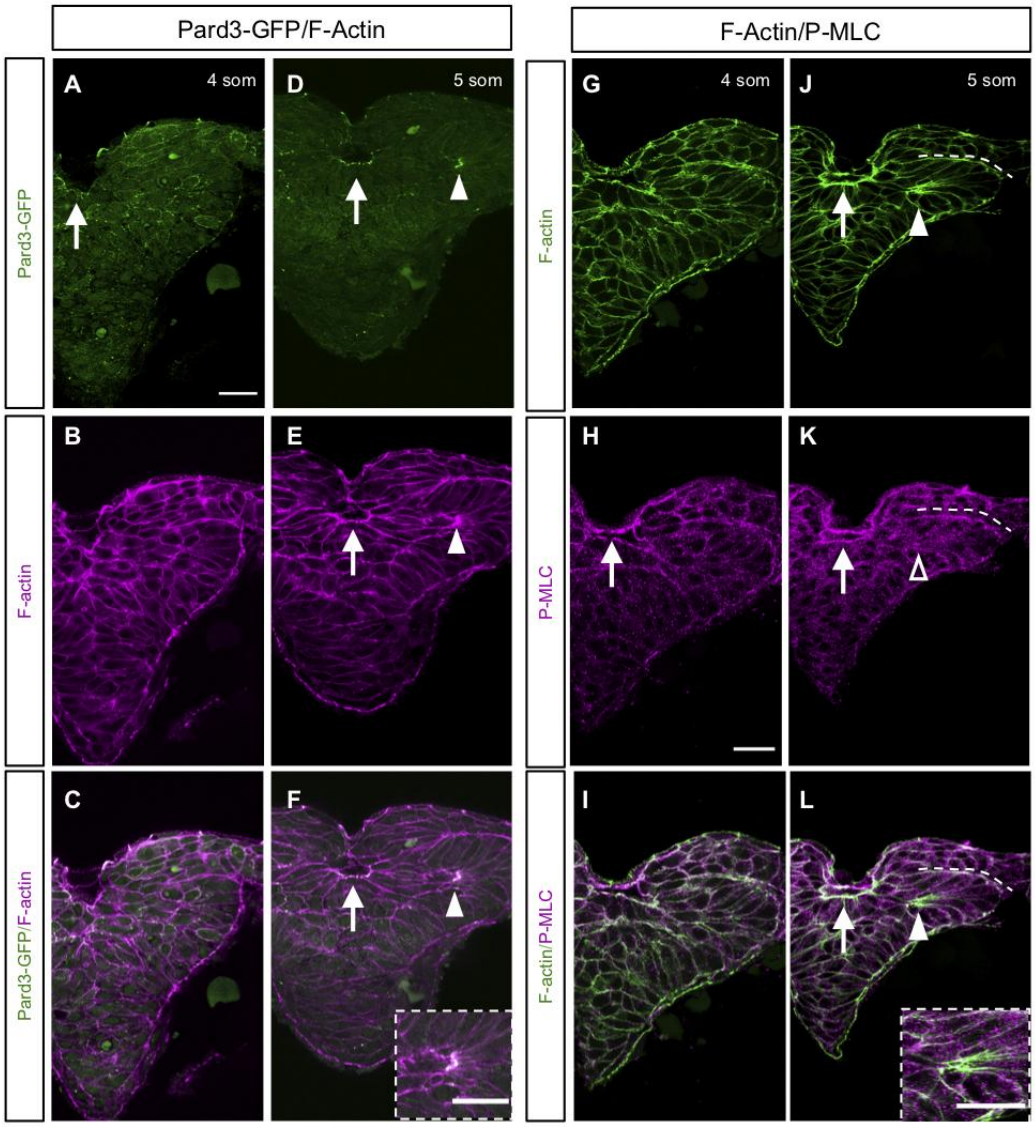

Figure 9. Molecular characterization of the MHP. (A-L). Transverse sections through the ANP at the 4 (A-C, G-I) and 5 (D-F, J-L) som stages. (A-F) Embryos double-labeled with Pard3-GFP (green) and phalloidin (F-actin, red) (G-L) Embryos double-labeled with anti-P-MLC (red) and phalloidin (F-actin, green).(C, F, I, L) Magenta and green channel overlay. Insets in F and L show higher magnification images of the DLHP. Annotations: arrow = MHP; arrowhead = DLHP; dotted line (in J-L) = interface between the NE and NNE layers of the neural folds. Scale bars 25 μm.

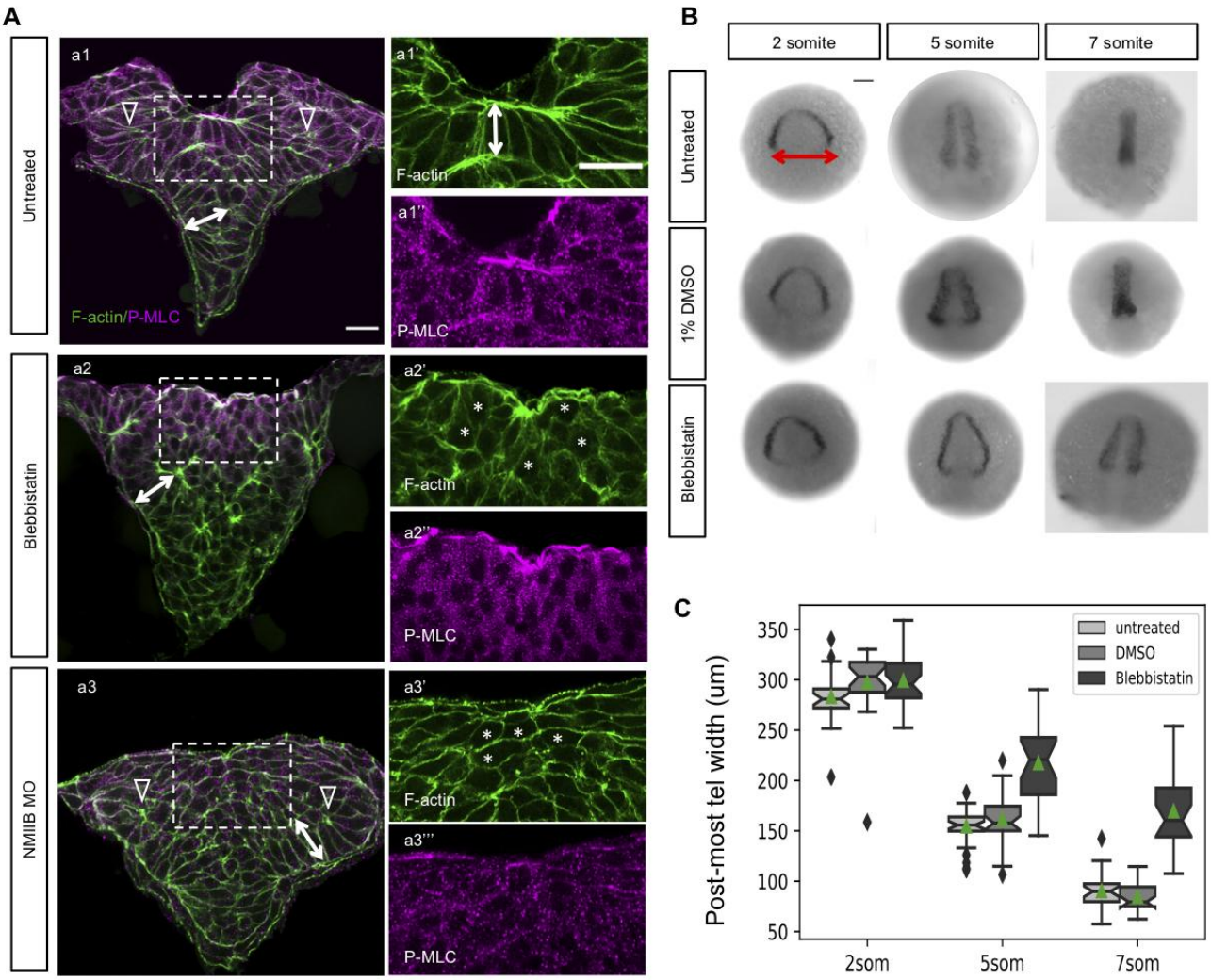

Figure 10. Role of non-muscle myosin II in apical constriction and neural fold convergence. (A). Transverse sections through the ANP of 5 som control, untreated (a1-a1''), blebbistatin-treated (a2-a2'') and *NMIIB* MO-injected (a3, a3', a3''). Embryos were double-labeled with phalloidin (F-actin,green) (A-F) and anti-P-MLC (red). (B) Dorsal views of 2, 5 and 7 som embryos untreated (top panels), DMSO-treated (middle row) and blebbistatin-treated (bottom row) labeled via *in situ* hybridization using an *emx3* riboprobe. (C) Boxplots showing distribution of posterior-most telencephalon widths (double red arrow in B) according to treatment group. Line in the middle of each boxplot is the median, notches around the median are 95% confidence intervals. Green triangles show the means. At least two independent experimental trials were performed for each developmental stage and treatment group. 2 som: Untreated: n=26, mean=283.224 ± 5.18; DMSO-treated: n= 26, mean=297.727 ± 6.41; blebbistatin-treated: n = 34, mean=299.412 ± 4.40. 5 som: Untreated: n=33, mean=154.688 ± 3.174; DMSO: n=30, mean=161.747 ± 4.73; blebbistatin-treated: n=23, mean=217.472 ± 8.43. Two-sided Mann Whitney U test: 5 som untreated vs DMSO: P=0.332; 5 som untreated vs blebbistatin-treated: P=1.30e^-7; 5 som DMSO-treated vs blebbistatin-treated: P = 3.50e^-6. 7 som: untreated: n=28, mean=90.444 ± 3.31; DMSO-treated: n=27, mean 84.855 ± 2.88; blebbistatin-treated: n=24, mean= 169.779 ± 7.52. Two-sided Mann Whitney U test: 7 som untreated vs DMSO: P=.170; 7 som untreated vs blebbistatin-treated: P=2.06e^-9; 7 som DMSO-treated vs blebbistatin-treated: P = 1.46e^-9. Annotations: double white arrows = cell length in deep layer; open arrowhead = DLHP; asterisks = rounded neuroectodermal cells; red double arrow = posterior-most telencephalon width. (a1'-a3'') Higher magnifications of boxed in areas in a1-a3. Scale bars: 25 μm in a1; 25 μm in a1' and 100 μm in B.

SUPPLEMENTARY FIGURE LEGENDS

Supplemental Figure 1. 3-Dimensional rotation revealing organization of neural fold cells in a 5 som embryo. Transverse section, at the level of the forebrain of a 5 somite embryo mosaically-expressing mGFP.

Supplemental Figure 2. 3-Dimensional rotation revealing organization of neural fold cells in a 7 som embryo. Transverse section, at the level of the forebrain of a 7 somite embryo mosaically-expressing mGFP.

Supplemental Figure 3. MHP cells undergo oscillatory constriction with decreasing amplitude. Time lapse imaging of embryo ubiquitously expressing mGFP. Clusters of medial (MHP) constrict apically in an oscillatory manner, in contrast to their lateral neighbors that do not. Annotations: cyan dots = MHP cells; yellow asterisks = MHP-adjacent cells that do not undergo apical constriction, yellow dashed line: midline, red asterisks = EVL cells.

Supplemental Figure 4. Neural tube closure is initiated at two closure points in the forebrain. Time lapse imaging of embryo mosaically-expressing mGFP. The Green and brightfield channels are overlaid to reveal the shape of the neural folds and neural groove. Annotations: red asterisk: apex of the arch shaped neural folds; white dotted line: contour of the eye-shaped opening whose corners are defined by closure points 1 and 2, double headed arrow: width of the neural plate, which decreases over time, white arrows: closure points 1 and 2, respectively.

Supplemental Figure 5. Neural fold cells extend filopodial protrusions across the midline. Time lapse imaging of embryo ubiquitously expressing mGFP. Cells (cyan and magenta) originating from contralateral sides of the ANP extend medially-oriented filopodia and transiently interdigitate across the midline (yellow dashed line).